*Chem. Mater.* **2007,** *19,* 1249−1256

# Development of Ruthenium−Hydroxyapatite-Encapsulated Superparamagnetic $\gamma$-$Fe_2O_3$ Nanocrystallites as an Efficient Oxidation Catalyst by Molecular Oxygen

Kohsuke Mori,[†] Satoko Kanai,[†] Takayoshi Hara,[†] Tomoo Mizugaki,[†] Kohki Ebitani,[†]
Koichiro Jitsukawa,[‡] and Kiyotomi Kaneda*[,†]

*Department of Materials Engineering Science, Graduate School of Engineering Science, Osaka University,1-3 Machikaneyama, Toyonaka, Osaka 560-8531, Japan, and Department of Materials Science and Engineering, Graduate School of Engineering, Nagoya Institute of Technology, Gokiso-cho, Showa-ku, Nagoya 466-8555, Japan*

*Received June 14, 2006. Revised Manuscript Received November 12, 2006*

Magnetic $\gamma$-$Fe_2O_3$ nanocrystallites dispersed in a hydroxyapatite matrix (HAP-$\gamma$-$Fe_2O_3$) have been synthesized for the first time as a new catalyst support. The cation-exchange ability of the external HAP surface enables an equimolar substitution of Ru for Ca to form a catalytically active center (RuHAP-$\gamma$-$Fe_2O_3$). Characterization by several spectroscopic methods demonstrated the formation of $\gamma$-$Fe_2O_3$ nanocrystallites within the HAP matrix having a mean diameter of 8.0 nm ($\sigma = 18.4$ Å, $\sigma/d = 21.7\%$). The Ru species was proven to exist in the monomeric form in a highly dispersed manner. The RuHAP-$\gamma$-$Fe_2O_3$ exhibits superior catalytic activity for the oxidation of various alcohols to the corresponding carbonyl compounds using molecular oxygen as a primary oxidant. The magnetic properties of the RuHAP-$\gamma$-$Fe_2O_3$ provided a convenient route for separation of the catalyst from the reaction mixture by application of an external permanent magnet. No metal leaching was detected, and the spent catalyst could be recycled without appreciable loss of catalytic activity.

## Introduction

An ongoing objective in the field of catalyst design is the development of innovative materials, in which the Ångstrom and nanoscale architecture of active centers plays a dominant role in determining their efficiency and selectivity.[1] For this purpose, molecular complexes, enzymes, metal nanoparticles, metal oxides, and periodic mesoporous materials have undergone extensive tuning in order to modify or expand their inherent properties. Another powerful method is to adopt a "bottom-up" construction approach to assemble the advantages of individual building blocks into integrated materials at the atomic/molecular level. The use of this protocol is expected to result in the discovery of new multifunctional materials, allowing for fascinating catalytic performances.[2]

Apatites—most notably hydroxyapatite (HAP), $Ca_{10}(PO_4)_6(OH)_2$—and related compounds are of considerable interest because of their structural stability and potential for cationic and anionic isomorphous substitutions.[3] The hexagonal apatite structure comprises $Ca^{2+}$ sites surrounded by tetrahedral $PO_4^{3-}$ units; $OH^-$ ions occupy columns parallel to the hexagonal axis. We have continuously explored novel nanostructured heterogeneous catalysts by utilization of promising ability of HAP, which can be considered as being a rigid macroligand for catalytically active centers.[4] For example, using a cation-exchange method, we have successfully created a versatile catalyst consisting of a stable monomeric Ru phosphate complex on the surface of HAP (RuHAP), which has excellent activity for selective oxidation reactions.[4a−c] Modification of the HAP surface is a powerful method for creating well-defined active sites, and also provides unexpected novel functions that cannot be achieved using molecular complexes.

We anticipated that the accommodation of magnetic nanocrystallites into the HAP matrix could generate a multifunctional catalyst combining prominent catalytic performances with magnetic properties, which could widen the application range of the HAP. The development of uniformly sized magnetic nanoparticles has been intensively pursued, and they have been exploited in the immobilization of

---

* Corresponding author. Phone and Fax: 81-6-6850-6260. E-mail: kaneda@cheng.es.osaka-u.ac.jp.
[†] Osaka University.
[‡] Nagoya Institute of Technology.

(1) (a) Anwander, R. *Chem. Mater.* **2001**, *13*, 4419. (b) De Vos, D. E.; Dams, M.; Sels, B. F.; Jacobs, P. A. *Chem. Rev.* **2002**, *102*, 3615. (c) Wight, A. P.; Davis, M. E. *Chem. Rev.* **2002**, *102*, 3589. (d) Argo, A. M.; Odzak, J. F.; Lai, F. S.; Gates, B. C. *Nature* **2002**, *415*, 623. (e) Copéret, C.; Chabanas, M.; Saint-Arroman, R. P.; Basset, J.-M. *Angew. Chem., Int. Ed.* **2003**, *42*, 156. (f) Kobayashi, S.; Akiyama, R. *Chem. Commun.* **2003**, 449.

(2) (a) Murugavel, R.; Walawalkar, M. G.; Dan, M.; Roesky, H. W.; Rao, C. N. R. *Acc. Chem. Res.* **2004**, *37*, 763. (b) Braunstein, P. *J. Organomet. Chem.* **2004**, *24*, 3953.

(3) Elliott, J. C. *Structure and Chemistry of the Apatites and Other Calcium Orthophosphates*; Elsevier: Amsterdam, 1994.

(4) (a) Yamaguchi, K.; Mori, K.; Mizugaki, T.; Ebitani, K.; Kaneda, K. *J. Am. Chem. Soc.* **2000**, *122*, 7144. (b) Mori, K.; Yamaguchi, K.; Hara, T.; Mizugaki, T.; Ebitani, K.; Kaneda, K. *J. Am. Chem. Soc.* **2002**, *124*, 11572. (c) Mori, K.; Hara, T.; Mizugaki, T.; Ebitani, K.; Kaneda, K. *J. Am. Chem. Soc.* **2003**, *125*, 11460. (d) Mori, K.; Hara, T.; Mizugaki, T.; Ebitani, K.; Kaneda, K. *J. Am. Chem. Soc.* **2004**, *126*, 10657.(e) Mori, K.; Oshiba, M.; Hara, T.; Mizugaki, T.; Ebitani, K.; Kaneda, K. *New J. Chem.* **2006**, *30*, 44.

10.1021/cm061388l CCC: $37.00

proteins, enzymes, bioactive agents, and metal complexes.[5] The fabrication of mesoporous silica and carbon materials incorporating magnetic nanoparticles has also been reported recently.[6] Among magnetic nanoparticles, $\gamma$-$Fe_2O_3$ (maghemite) is a technologically important material because of its crucial role in catalysis and in the formation of magnetic storage media.[7] This report describes our detailed studies of the synthesis and characterization of ruthenium−hydroxyapatite encapsulated magnetic $\gamma$-$Fe_2O_3$ (RuHAP-$\gamma$-$Fe_2O_3$) and its evaluation as a heterogeneous catalyst for the oxidation of alcohol using molecular oxygen. We found a significant improvement in the catalytic activity of the RuHAP-$\gamma$-$Fe_2O_3$ in comparison to the previously reported RuHAP catalyst. We also discuss some interesting aspects such as substrate scope and magnetic recyclability, as well as mechanistic investigations. To the best of our knowledge, this is the first demonstration of an apatite catalyst with magnetic properties.

## Experimental Section

**Materials.** $RuCl_3 \cdot xH_2O$ was obtained from N. E. Chemcat Co. Ltd. and used without further purification. $FeCl_2 \cdot 4H_2O$, $FeCl_3 \cdot 6H_2O$, $(NH_4)_2HPO_4$, and $Ca(NO_3)_2 \cdot 4H_2O$ were purchased from Wako Pure Chemical Ind., Ltd. Solvents and all commercially available alcohols were purified by standard procedures used before.

**Synthesis of Ruthenium-Exchanged Hydroxyapatite-Encapsulated Magnetic $\gamma$-$Fe_2O_3$ (RuHAP-$\gamma$-$Fe_2O_3$).** $FeCl_2 \cdot 4H_2O$ (1.85 mmol) and $FeCl_3 \cdot 6H_2O$ (3.7 mmol) were dissolved in deoxygenated water (30 mL) under an Ar atmosphere at room temperature, and the resulting solution was added to a 25% $NH_4OH$ solution (10 mL) under vigorous mechanical stirring (300 rpm). A black precipitate was produced instantly. After 15 min, 100 mL of $Ca(NO_3)_2 \cdot 4H_2O$ (33.7 mmol, 0.5 M) and $(NH_4)_2HPO_4$ (20 mmol, 30 M) solutions whose pH were adjusted to 11 were added dropwise to the obtained precipitate solution over 30 min with mechanical stirring, respectively, and the resulting milky solution was heated at 90 °C. After 2 h, the mixture was cooled to room temperature and aged overnight without stirring. The obtained precipitate was filtered, washed repeatedly with deionized water till neutrality, and air-dried at room temperature. The as-synthesized sample was calcined at 200 °C for 3 h, giving a reddish-brown powder (Anal. Calcd: Ca, 35.3; P, 16.4; Fe, 8.1 wt %. Found: Ca, 35.5; P, 16.3; Fe, 8.2 wt %.). Treatment of the above powder (1.0 g) with 100 mL of an aqueous $RuCl_3 \cdot xH_2O$ solution ($1.0 \times 10^{-3}$ M) at room temperature for 24 h, followed by filtration and drying under a vacuum overnight, yielded a black powder (Anal. Calcd: Ca, 29.5; P, 15.4; Fe, 7.6; Ru, 1.0 wt %. Found: Ca, 29.4; P, 15.12; Fe, 8.0; Ru, 1.0 wt %.).

**Typical Example for the Oxidation of Alcohols.** Into a reaction vessel with a reflux condenser were placed RuHAP-$\gamma$-$Fe_2O_3$ (0.05 g, Ru: 0.5 mol %), benzyl alcohol (1 mmol), and toluene (5 mL). The resulting mixture was stirred at 90 °C under $O_2$ flow conditions (ca. 1 mL/min). The progress of the reaction was monitored by GC analysis using an internal standard technique. After 1 h, a 98% yield of benzaldehyde was obtained. The isolated catalyst was washed with 10 mL of toluene and 10 mL of an aqueous NaOH solution ($1.0 \times 10^{-2}$ M) before reuse. The recycling procedures were repeated in the same manner as in the first run. The amount of $O_2$ uptake was volumetrically measured by a gas buret directly connected to the rotary vacuum pump.

**Characterization.** Analytical GC was performed by a Shimadzu GC-8AP and GC-1700 with flame ionization detector equipped with KOCL300T, Silicone UC W-98, Silicone OV-17 columns. BET surface area measurement was performed with BELSORP 18PLUS-SP analyzer (BEL Japan, Inc.) at 77 K. The sample was degassed in a vacuum at 130 °C prior to data collection. Powder X-ray diffraction patterns were recorded using Philips X'Pert-MPD with Cu K$\alpha$ radiation of wavelength 1.5418 Å. X-ray photoelectron spectroscopy was measured on Shimadzu ESCA-KM using Mg K$\alpha$ radiation. Powder samples were pressed to be attached on carbon tape and mounted on a sample folder. Binding energy was calibrated using the $C_{1s}$ photoelectric peak at 285.0 eV. Infrared spectra were obtained with a JASCO FTIR-410 instrument. Samples were diluted with KBr and compressed into thin disk-shaped pellets. Inductively coupled plasma measurements were performed by Nippon Jarrell-Ash ICAP-575 Mark II instrument. Magnetic properties were measured with a Quantum Design MPMS-XL instrument. Field-cooled (FC) and zero-field-cooled (ZFC) runs were completed in the temperature range of $5 \text{ K} \leq T \leq 300 \text{ K}$ under $H = 100$ Oe. $^{57}Fe$ Mössbauer spectra were obtained with a conventional spectrometer in a transmission geometry. $^{57}Co$ in Rh was used for a $\gamma$-ray source, and the velocity scale is relative to $\alpha$-Fe at room temperature. X-ray absorption spectra were recorded using a fluorescence-yield collection technique at the beam line 01B1 station with attached Si (311) monochromator at SPring-8, JASRI, Harima, Japan (prop. 2005A0694-NXa-np). The EXAFS data were normalized by fitting the background absorption coefficient around the energy region higher than the edge by about 35−50 eV with the smoothed absorption of an isolated atom. The EXAFS data were examined by an EXAFS analysis program, Rigaku EXAFS. Fourier transformation (FT) of $k^3$-weighted normalized EXAFS data was performed over the $3.5 \text{ Å} < k/\text{Å}^{-1} < 12 \text{ Å}$ range to obtain the radial structure function. CN (coordination number of scatters), $R$ (distance between an absorbing atom and scatterer), and Debye−Waller factor were estimated by curve-fitting analysis with the inverse FT of the $0.8 < R/\text{Å} < 2.8$ range assuming single scattering. HR-TEM micrographs were obtained with a Hitachi Hf-2000 FE-TEM instrument equipped with a Kevex energy-dispersive X-ray detector operated at 200 kV.

## Results and Discussion

**Catalyst Preparation and Characterization.** Our previously reported Ru−hydroxyapatite (RuHAP, Ru content: 1.7 mmol/g) was prepared by simple treatment of the stoichiometric HAP, $Ca_{10}(PO_4)_6(OH)_2$, with an aqueous solution of $RuCl_3 \cdot xH_2O$ at room temperature.[4a] Characterization by various physicochemical methods demonstrated that an equimolar substitution of Ru for Ca had taken place on the HAP surface, generating a monomeric $RuCl^{2+}$ species surrounded by four oxygen atoms. More recently, Baiker and co-workers developed a Co-promoted Ru−hydroxyapatite (RuCo-HAP) by fine-tuning the local environment of the active Ru site, i.e., by lowering the Ru content (0.34 mmol/

---

(5) (a) Laslie-Pelecky, D. L.; Rieke, R. D. *Chem. Mater.* **1996**, *8*, 1770. (b) Hyeon, T. *Chem. Commun.* **2003**, 927.

(6) (a) Garcia, C.; Zhang, Y.; DiSalvo, F.; Wiesner, U. *Angew. Chem., Int. Ed.* **2003**, *42*, 1526. (b) Lu, A.-H.; Schmidt, W.; Matoussevitch, N.; Bönneman, H.; Spliethoff, B.; Tesche, B.; Bill, E.; Kiefer, W.; Schüth, F. *Angew. Chem., Int. Ed.* **2004**, *43*, 4303. (c) Tsang, S. C.; Caps, V.; Paraskevas, I.; Chadwick, D.; Thompsett, D. *Angew. Chem., Int. Ed.* **2004**, *43*, 5645.

(7) (a) Sugimoto, M. *J. Am. Ceram. Soc.* **1999**, *82*, 269. (b) Bate, G. *J. Magn. Magn. Mater.* **1999**, *100*, 413.

g) and incorporating Co cations.[8] This RuCo-HAP showed high catalytic activity compared to the classically prepared RuHAP in the oxidation of alcohols using molecular oxygen. On the basis of various methods of characterization, it is thought that the active site consists of $Ru(OH)_2^{2+}$ surrounded by four oxygen atoms.[8b] As part of our ongoing project designing high-performance heterogeneous catalysts, we focused on the development of a novel Ru-based hydroxyapatite catalyst, which has the advantage of greater operational simplicity as well as enabling unprecedented catalytic activity in the aerobic oxidation of alcohols.

$\gamma$-$Fe_2O_3$ nanocrystallites are commonly synthesized by coprecipitation of ferrous ($Fe^{2+}$) and ferric ($Fe^{3+}$) ions in a basic aqueous solution followed by thermal treatment,[9] or by thermal decomposition of iron precursors such as $Fe(CO)_5$ and $Fe(NO_3)_2$.[10] We employed the coprecipitation approach because basic aqueous conditions allow for subsequent crystallization of the HAP phase and further coating of the $\gamma$-$Fe_2O_3$ nanocrystallites with HAP. The synthetic procedure for ruthenium–hydroxyapatite-encapsulated magnetic $\gamma$-$Fe_2O_3$ (RuHAP-$\gamma$-$Fe_2O_3$) is as follows. A mixture of the ferrous and ferric salt solutions ($Fe^{2+}/Fe^{3+} = 0.5$) was introduced into an $NH_4OH$ solution at room temperature. To the resulting black nanoparticles solution were added aqueous solutions of $Ca(NO_3)_2 \cdot 4H_2O$ and $(NH_4)_2HPO_4$ dropwise with vigorous mechanical stirring. The resultant milky solution was heated at 90 °C to produce a black powder, which was calcined at 200 °C to give hydroxyapatite-encapsulated magnetic $\gamma$-$Fe_2O_3$ (HAP-$\gamma$-$Fe_2O_3$) as a reddish-brown powder. The Ca/P ratio of the HAP-$\gamma$-$Fe_2O_3$ was estimated to be 1.67, in agreement with the stoichiometric value of the hydroxyapatite. Subsequently, treatment of the HAP-$\gamma$-$Fe_2O_3$ with an aqueous $RuCl_3 \cdot xH_2O$ solution yielded the RuHAP-$\gamma$-$Fe_2O_3$ as a black powder (Ru: 1.0 wt %, 0.1 mmol/g). The (Ru + Ca)/P ratio of the RuHAP-$\gamma$-$Fe_2O_3$ was determined to be ca. 1.67.

The $N_2$ adsorption–desorption isotherm of the RuHAP-$\gamma$-$Fe_2O_3$ showed a gradual increase in the amount of adsorbed $N_2$ without a hysteresis loop (Figure 1). According to the IUPAC, it can be classified as a type III isotherm, reflecting the absence of micropores (<2 nm). The Brunauer–Emmett–Teller (BET) surface area was found to be 115.4 $m^2\ g^{-1}$, which is considerably larger than that of the previously reported RuHAP (49.6 $m^2\ g^{-1}$). This result suggests that the crystal growth of the HAP phase was suppressed during the present preparation sequences. The infrared spectrum (IR) of the RuHAP-$\gamma$-$Fe_2O_3$ was similar to that of the parent HAP, confirming the formation of the HAP phase.[11]

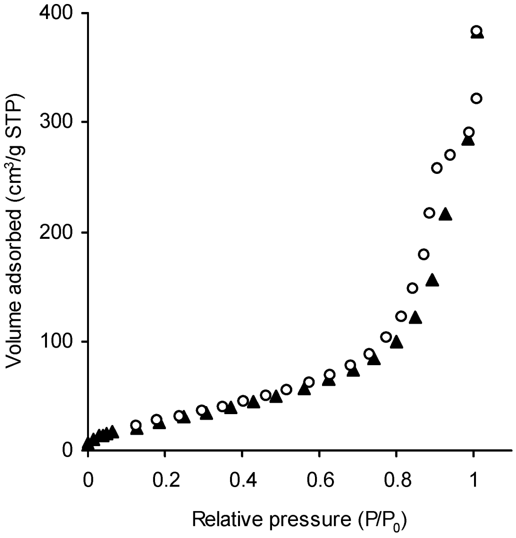

**Figure 1.** $N_2$ adsorption (▲)–desorption (○) isotherm for RuHAP-$\gamma$-$Fe_2O_3$.

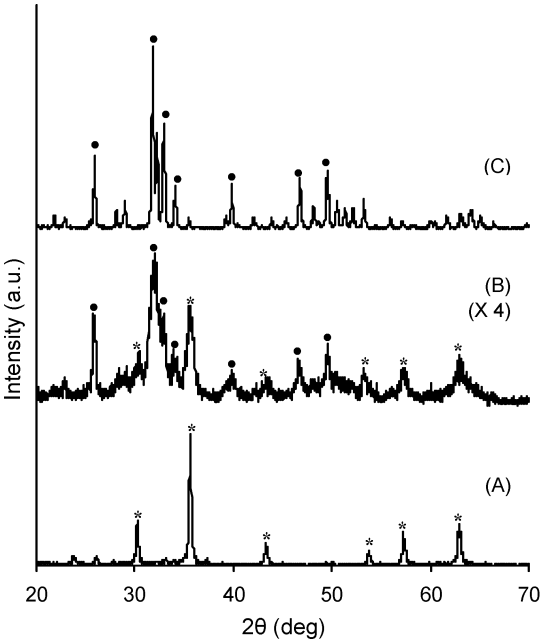

**Figure 2.** XRD patterns of (A) $\gamma$-$Fe_2O_3$, (B) RuHAP-$\gamma$-$Fe_2O_3$, and (C) HAP.

The powder X-ray diffraction (XRD) patterns of the RuHAP-$\gamma$-$Fe_2O_3$, together with those of the original HAP and $\gamma$-$Fe_2O_3$ crystallites as reference samples, are shown in Figure 2. The intensity of diffraction peaks for the RuHAP-$\gamma$-$Fe_2O_3$ is low, presumably due to the smaller size of the particles. However, it exhibited clear peaks due to the HAP lattice along with $\gamma$-$Fe_2O_3$ phase at around 30.2, 35.7, 43.6, 53.6, 57.3, and 63.0°, corresponding to the (220), (311), (400), (422), (511), and (440) reflections, respectively. The average crystalline size of $\gamma$-$Fe_2O_3$ was calculated to be 9.1 nm by applying Scherrer's equation for (311) reflection. Other iron oxide phases such as $\alpha$-$Fe_2O_3$ and metallic bcc Fe nanoparticles are apparently not involved. The Raman spectrum, which is often applied as a useful technique for

---

(8) (a) Opre, Z.; Grunwaldt, J.-D.; Maciejewski, M.; Ferri, D.; Mallat, T.; Baiker, A. *J. Catal.* **2005**, *230*, 415. (b) Opre, Z.; Grunwaldt, J.-D.; Mallat, T.; Baiker, A. *J. Mol. Catal., A* **2005**, *242*, 224.

(9) The coprecipitation of ferrous ($Fe^{2+}$) and ferric ($Fe^{3+}$) ions in a basic aqueous solution gives $Fe_3O_4$ nanoparticles, which can be directly oxidized into $\gamma$-$Fe_2O_3$ under air conditions, see (a) Kang, Y. S.; Risbud, S.; Rabolt, J. F.; Stroeve, P. *Chem. Mater.* **1996**, *8*, 2209. (b) Zhang, L.; Papaefthymiou, G. C.; Ziolo, R. F.; Ying, J. Y. *Nanostruct. Mater.* **1997**, *9*, 185. (c) Chakrabari, S.; Mandal, S. K.; Nath, B. K.; Das, D.; Ganguli, D.; Chaudhuri, S. *Eur. Phys. J. B* **2003**, *34*, 163.

(10) (a) Hyeon, T.; Lee, S. S.; Park, J.; Chung, Y.; Na, H. B. *J. Am. Chem. Soc.* **2001**, *123*, 12798. (b) Cannas, C.; Concas, G.; Gatteschi, D.; Falqui, A.; Musinu, A.; Piccaluga, G.; Sangregorio, C.; Spano, G.; *Phys. Chem. Chem. Phys.* **2001**, *3*, 832. (c) Zhang, L.; Papaefthymiou, G. C.; Ying, J. Y. *J. Phys. Chem. B* **2001**, *105*, 7414.

(11) See the Supporting Information.

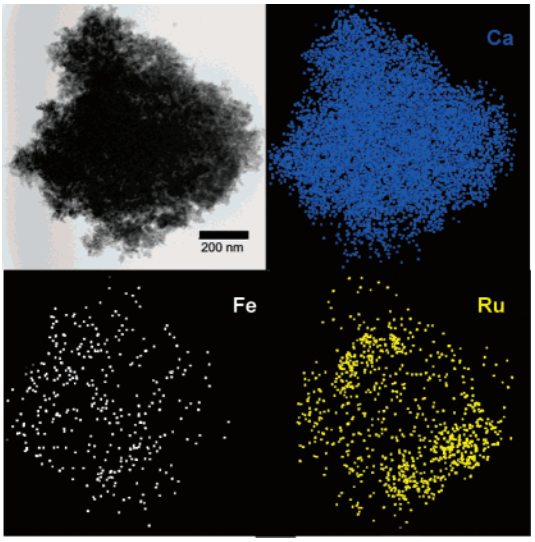

**Figure 3.** TEM image of RuHAP-$\gamma$-$Fe_2O_3$ and STEM elemental mappings.

differentiating various iron oxide phases, matched with the reported $\gamma$-$Fe_2O_3$ phase.[11,12] Evidence for the formation of $\gamma$-$Fe_2O_3$ was also shown by X-ray photoelectron spectroscopy (XPS): the positions of the $Fe2p_{3/2}$ and $Fe2p_{1/2}$ peaks in the RuHAP-$\gamma$-$Fe_2O_3$ were 711.3 and 724.9 eV, which is in good agreement with the peaks of $\gamma$-$Fe_2O_3$ but differs from those of $Fe_3O_4$ by ~1 eV.[13] No metallic Fe signals were detected in the XPS spectra.

$\gamma$-$Fe_2O_3$ crystallites were not observed in the scanning electron microscopy (SEM) image of RuHAP-$\gamma$-$Fe_2O_3$, which is possibly due to the smaller size of the nanocrystallites.[11] The scanning transmission electron microscopy (STEM) image with elemental mapping is depicted in Figure 3. This showed that both Fe and Ru species were virtually highly dispersed throughout the image area, but an uneven distribution area might exist in the sample because the dispersions of these elements were not the same. Figure 4 shows a high-resolution transmission electron microscopy (HR-TEM) image and size distribution diagram. The $\gamma$-$Fe_2O_3$ nanocrystallites having a mean diameter ($d$) of ca. 8.0 nm were found to be distributed within the host HAP matrix (standard deviation: $\sigma$ = 18.4 Å, $\sigma/d$ = 21.7%). The diffraction patterns (**B** in Figure 4) exhibited atomic lattice fringes corresponding to the (220), (311), and (400) planes of $\gamma$-$Fe_2O_3$, respectively, which is consistent with the results of XRD and XPS analyses as described earlier.[10a]

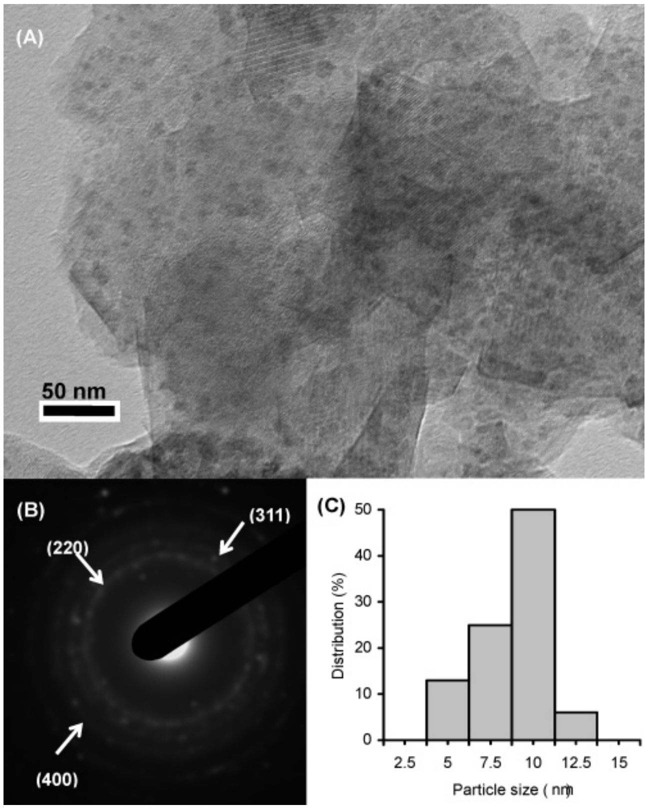

**Figure 4.** (A) HRTEM image, (B) electron diffraction pattern, and (C) size distribution diagram for the RuHAP-$\gamma$-$Fe_2O_3$.

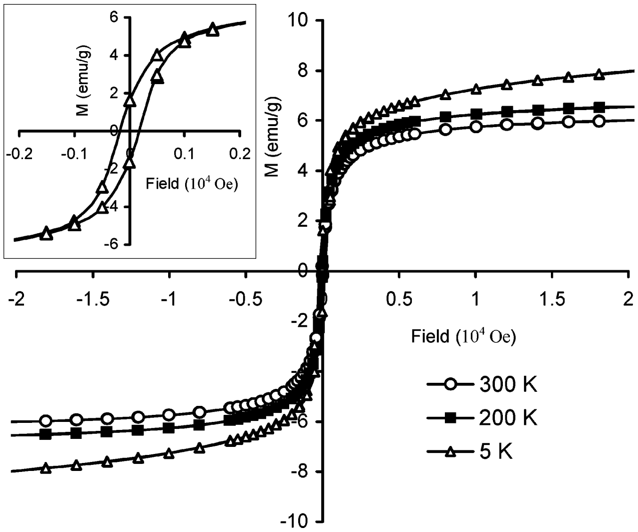

**Figure 5.** Field-dependent magnetization curve for RuHAP-$\gamma$-$Fe_2O_3$ measured at 300 (○), 200 (■), and 5 (Δ). Inset shows low field region of the hysteresis loop measured at 5 K.

The magnetic properties of the RuHAP-$\gamma$-$Fe_2O_3$ were investigated using a superconducting quantum interface device (SQUID) magnetometer. As shown in Figure 5, the isothermal magnetization curve of the RuHAP-$\gamma$-$Fe_2O_3$ at 300 K displayed a rapid increase with increasing applied magnetic field due to superparamagnetic relaxation.[14] Hysteresis was absent with zero remanence and coercivity, and the saturation magnetization ($M_s$) reached up to 6.0 emu/g. When normalized to the $\gamma$-$Fe_2O_3$ content in the sample, the $M_s$ of 55 emu/g for $\gamma$-$Fe_2O_3$ in the HAP matrix was smaller than the theoretical $M_s$ of 76 emu/g for bulk $\gamma$-$Fe_2O_3$ at room temperature.[15] This difference can be explained by the defined size effects responsible for the degradation of magnetic properties in iron oxide nanocrystallites.[16]

With decreasing temperature, the magnetization of the sample increased and exhibited a symmetric hysteresis loop at 5K, indicating a transition from superparamagmetic to ferrimagnetic behavior. As shown in Figure 6, the zero-field-

---

(12) Pascal, C.; Pascal, J. L.; Favier, F.; Moubtassim, M. L. E.; Payen, C. *Chem. Mater.* **1999**, *11*, 141.

(13) Teng, X.; Black, D.; Watkins, N. J.; Gao, Y.; Yang, H. *Nano Lett.* **2003**, *3*, 261.

(14) Coey, J. M.; Khalafalla, D. *Phys. Status Solidi A* **1972**, *11*, 229.

(15) Cullity, B. D. *Introduction to Magnetic Materials*; Addison-Wesley: Reading, MA, 1972; p 201.

(16) Craik, D. J. *Magnetic Oxides*; Wiley: New York, 1975; p 697.

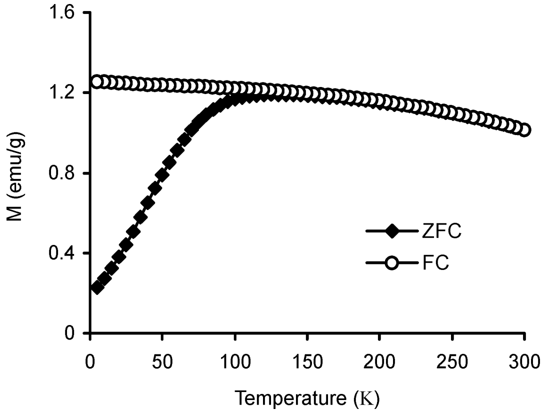

**Figure 6.** ZFC and FC magnetization curve for RuHAP-$\gamma$-$Fe_2O_3$ measured under 100 Oe.

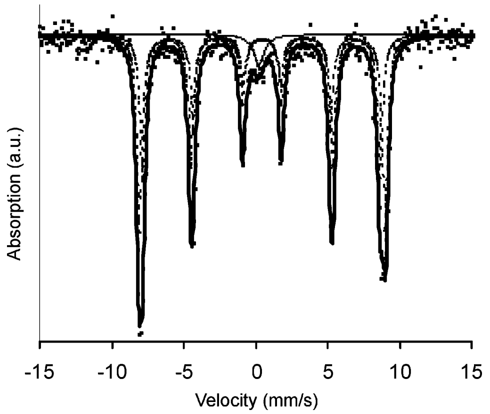

**Figure 7.** Mössbauer spectrum (dot) and simulated spectrum (solid line) of the RuHAP-$\gamma$-$Fe_2O_3$ at 5 K.

**Table 1. Analyzed Results of the Mössbauer Spectrum**

| fitted spectrum | IS (mm/s) | Hf (T) | QS (mm/s) | area (%) | Fe ion state |
|---|---|---|---|---|---|
| sextet | 0.47 | 53 | 0.02 | 55 | +3 |
| sextet | 0.42 | 51 | −0.04 | 41 | +3 |
| single | 0.22 | | | 4 | +3 |

cooled (ZFC) and field-cooled (FC) magnetization under an applied field of 100 Oe between 5 and 300 K gave further confirmation of superparamagnetism of the nanoparticles. They exhibited the behavior of superparamagmetic $\gamma$-$Fe_2O_3$ nanoparticles with some interactions among the particles. The blocking temperature ($T_B$) was determined to be 140 K, which was comparable to that of $\gamma$-$Fe_2O_3$ nanoparticles with the mean diameter of 8.0 nm determined by HR-TEM analysis; it has been reported that the $T_B$ values of the $\gamma$-$Fe_2O_3$ nanoparticles with particles diameters of 4, 9, and 10 nm were found to be 25, 150, and 175, respectively.[10a,17]

Figure 7 shows the $^{57}$Fe Mössbauer spectra at 5 K. The original data was fitted into a singlet and two sextet patterns, as summarized in Table 1. The values of isomer shift (IS), hyperfine field (Hf), and quadruple splitting (QS) of two sextets were determined to be 0.47 and 0.42 mm/s, 53 and 51 T, and 0.02 and −0.04 mm/s, respectively. The IS value smaller than 0.5 mm/s suggested $Fe^{3+}$ ion. These parameters clearly indicate that the $Fe^{2+}$ ion is absent and that the phase formed is maghemite ($\gamma$-$Fe_2O_3$).

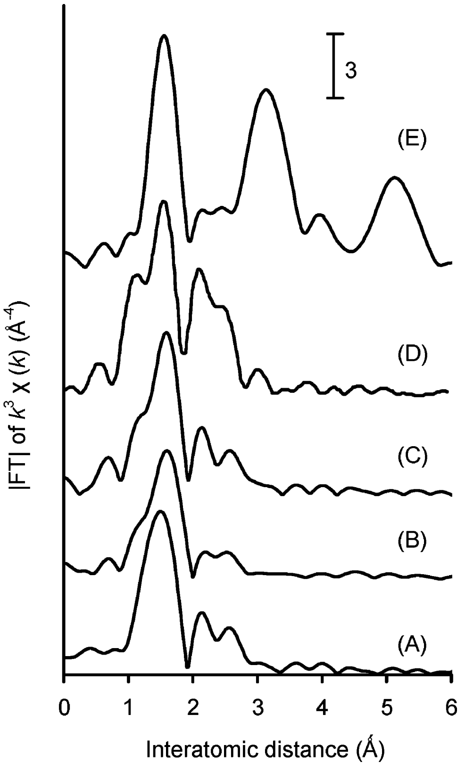

**Figure 8.** Fourier-transforms of $k^3$-weighted Ru K-edge EXAFS experimental data for (A) fresh RuHAP-$\gamma$-$Fe_2O_3$, (B) RuHAP-$\gamma$-$Fe_2O_3$ reacted under an Ar atmosphere with benzyl alcohol, (C) after the reaction of (B) with $O_2$, (D) RuHAP, and (E) $RuO_2$.

To gain insight into the local environment of the Ru species in the RuHAP-$\gamma$-$Fe_2O_3$ framework, we carried out characterization by means of XPS and Ru K-edge EXAFS. The binding energy of the $Ru3p_{3/2}$ in the RuHAP-$\gamma$-$Fe_2O_3$ is 465.2 eV, which is similar to the value of 465.0 eV for $Ru^{IV}Cl_6(NH_4)_2$ and higher than the value of 463.8 eV for the classically prepared RuHAP involving $Ru^{III}$ species. This reveals the occurrence of electron transfer from Ru to the HAP-$\gamma$-$Fe_2O_3$ support and the generation of a higher oxidation state of the $Ru^{IV}$ species in the RuHAP-$\gamma$-$Fe_2O_3$. Electron transfer from metals to $\gamma$-$Fe_2O_3$ has previously been reported in the Pt/$\gamma$-$Fe_2O_3$[18] and Ru/$\gamma$-$Fe_2O_3$[19] nanocomposites, as evidenced by XPS analysis.[20]

The Ru K-edge X-ray absorption near-edge structure (XANES) spectrum of the RuHAP-$\gamma$-$Fe_2O_3$ was identical to that of $RuO_2$, but differed from those of Ru metal, $RuCl_2(PPh_3)_3$, and $RuCl_6(NH_4)_2$. The Fourier transforms (FT) of $k^3$-weighted extended X-ray absorption fine structure (EXAFS) data are depicted in Figure 8. There were no peaks in the RuHAP-$\gamma$-$Fe_2O_3$, suggestive of contiguous Ru−O−Ru bonds (**A**), as detected for $RuO_2$ (**E**) at around 3.5 Å. The intensity of the peak at around 2.2 Å, attributable to the Ru−Cl bond, was lower than that of RuHAP (**D**). The inverse FT of the main peaks was well-fitted, using only a Ru−O

---

(17) Mukadam, M. D.; Yusuf, S. M.; Sharma, P.; Kulshreshtha, S. K. *J. Magn. Magn. Mater.* **2004**, *272−276*, 1401.

(18) Zhang, J.; Wang, Y.; Ji. H.; Wei, Y.; Wu, N.; Zuo, B.; Wang, Q. *J. Catal.* **2005**, *229*, 114.

(19) Helgason, Ö.; Greneche, J.-M.; Berry, F. J.; Mosselmans, F. *J. Phys.: Condens. Matter.* **2003**, *15*, 2907.

(20) The oxidation of Ru(III) to Ru(IV) has also been observed by lowering the Ru content using solid base support. See Motokura, K.; Nishimura, D.; Mori, K.; Mizugaki, T.; Ebitani, K.; Kaneda, K. *J. Am. Chem. Soc.* **2004**, *126*, 5662.

bond with an interatomic distance (*R*) of 1.95 Å and a coordination number (CN) of 6, respectively. These are assigned to Ru−OH and Ru−O−P moieties. The Ru=O species with a shorter bond distance (ca. 1.85 Å) may not be involved.[21] Considering the above results, we propose that the Ru species on the RuHAP-$\gamma$-$Fe_2O_3$ surface is a monomeric $Ru(OH)_2^{2+}$ surrounded by four phosphate ligands. The proposed surface Ru species differs from that of our previously reported RuHAP.[4a] Presumably, lowering of the Ru content and incorporation of $\gamma$-$Fe_2O_3$ nanocrystallites might have an affect on the local environment of the active Ru species. Conclusively, we succeeded in designing Ru−hydroxyapatite-encapsulated magnetic $\gamma$-$Fe_2O_3$ nanocrystallites as a multifunctional nanomaterial possessing both active Ru species and magnetic properties. The use of the HAP matrix as a host can provide an effective way for tailoring a uniform particle size and homogeneous dispersion of magnetic $\gamma$-$Fe_2O_3$ nanocrystallites, while retaining the multiple functionalities of HAP.

**Aerobic Oxidation of Alcohols Using the RuHAP-$\gamma$-$Fe_2O_3$ Catalyst.** The selective oxidation of alcohols is widely recognized as one of the most fundamental transformations in both laboratory and industrial synthetic chemistry, because the resulting carbonyl compounds are of paramount importance as synthetic intermediates for fine chemicals and pharmaceuticals.[22] Due to ever-growing environmental concerns, there is a strong need for the establishment of promising catalytic protocols using molecular oxygen as a sole oxidant, which is readily available and produces only water as a byproduct.[23] Accordingly, a remarkable number of Pd-, Ru-, and Cu-catalyzed aerobic processes, both homogeneous and heterogeneous, have been developed in recent years.[24]

We explored the potential catalytic ability of the RuHAP-$\gamma$-$Fe_2O_3$ in the oxidation of alcohols using molecular oxygen. As can be seen from Table 2, various benzylic, allylic, and aliphatic alcohols were selectively converted into the corresponding carbonyl compounds with excellent yields under 1 atm of $O_2$ pressure. In particular, benzylic and allylic alcohols showed high reactivity for oxidative dehydrogenation (entries 1−12). A 10 mmol-scale oxidation of benzyl alcohol was also performed, giving benzaldehyde in 93% yield; the turnover number (TON) based on Ru approached 930 after 24 h. In the case of cyclopropylphenyl carbinol, oxidation of the hydroxyl group occurred without cleavage of the cyclopropyl ring (entry 9). In the oxidation of cinnamyl alcohol, C=C double bonds remained intact without an intramolecular hydrogen transfer (entries 11). A primary aliphatic alcohol, 1-dodecanol, was successfully oxidized, affording 1-dodecanoic acid without any formation of the corresponding aldehyde and ester (entry 13). The RuHAP-$\gamma$-$Fe_2O_3$ catalyst was effective in the oxidation of heterocyclic alcohols such as 2-pyridinemethanol and 2-thiophenemethanol, affording the corresponding aldehydes in high yields (entries 19 and 21). In general, the previously reported homogeneous monomeric transition metal complexes are unable to catalyze the oxidation of these alcohols containing heteroatoms, because their strong coordination to the metal center causes catalyst deactivation. The RuHAP-$\gamma$-$Fe_2O_3$ catalyst was also found to be applicable to the oxidation of sterically bulky alcohols: 3,5-dibenzyloxybenzyl alcohol and cholestanol were successfully converted into the corresponding carbonyl compounds with excellent yields, respectively (eqs 1 and 2). In particular, the oxidation of 7-hexadecyn-1-ol proceeded quantitatively without any effect on the alkynyl group (eq 3). These oxidation results confirm the absence of micropores, as shown by the $N_2$ adsorption−desorption isotherm, and that the active Ru species are located dominantly on the catalyst surface.

**Table 2. Oxidation of Various Alcohols Catalyzed by RuHAP-$\gamma$-$Fe_2O_3$ under 1 and 5 atm of Molecular Oxygen[a]**

| entry | substrate | $O_2$ pressure [atm] | time [h] | conv. [%][b] | yield [%][b] | TOF [$h^{-1}$] |
|---|---|---|---|---|---|---|
| 1 | 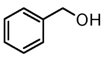 | 1 | 1 | >99 | 98 | 196 |
| 2 | | 5 | 0.5 | >99 | 94 | 376 |
| 3 | 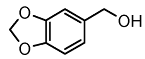 | 1 | 2 | >99 | 99 | 99 |
| 4 | | 5 | 1 | >99 | 99 | 198 |
| 5 | 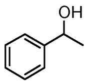 | 1 | 2 | 95 | 91 | 91 |
| 6 | | 5 | 1 | 95 | 95 | 160 |
| 7 | 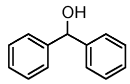 | 1 | 1 | >99 | 98 | 196 |
| 8 | | 5 | 0.5 | >99 | 98 | 392 |
| 9 | 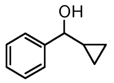 | 1 | 6 | >99 | >99 | 33 |
| 10 | | 5 | 3 | >99 | 96 | 64 |
| 11[c] | 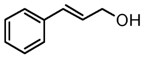 | 1 | 2.5 | 91 | 86 | 34 |
| 12[c] | | 5 | 1.25 | >99 | 96 | 77 |
| 13[d] | 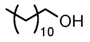 | 1 | 9 | >99 | 98[e] | 11 |
| 14[d] | | 5 | 9 | >99 | >99[e] | 11 |
| 15[d] | 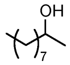 | 1 | 12 | 87 | 83 | 7 |
| 16[d] | | 5 | 10 | 92 | 91 | 9 |
| 17 | 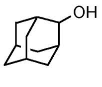 | 1 | 2 | >99 | >99 | 100 |
| 18 | | 5 | 1 | 89 | 81 | 162 |
| 19[c] | 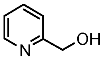 | 1 | 15 | 89 | 88 | 6 |
| 20[c] | | 5 | 15 | 95 | 95 | 6 |
| 21[c] | 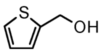 | 1 | 5 | >99 | 96 | 19 |
| 22[c] | | 5 | 2.5 | >99 | 98 | 39 |

[a] Alcohol (1 mmol), RuHAP-$\gamma$-$Fe_2O_3$ (0.5 mol %), toluene (5 mL), 90 °C, $O_2$ flow. [b] Determined by GC using an internal standard technique. [c] RuHAP-$\gamma$-$Fe_2O_3$ (1 mol %). [d] RuHAP-$\gamma$-$Fe_2O_3$ (1 mol %), α,α,α,-trifluorotoluene (5 mL). [e] 1-Octanoic acid was formed.

---

(21) Ji, H.-B.; Ebitani, K.; Mizugaki, T.; Kaneda, K. *Catal. Commun.* **2002**, *3*, 511.

(22) (a) Sheldon, R. A.; Kochi, J. K. *Metal-Catalyzed Oxidations of Organic Compounds*; Academic Press: New York, 1981. (b) Hill, C. L. *Advances in Oxygenated Processes*; Baumstark, A. L. Ed.; JAI Press, Inc.: London, 1988; Vol. 1, p 1. (c) Hudlucky, M. *Oxidations in Organic Chemistry*; ACS Monograph Series; American Chemical Society: Washington, D.C., 1990. (d) *Comprehensive Organic Synthesis*; Trost, B. M., Fleming, I., Eds.; Pergamon: Oxford, U.K., 1991.

(23) (a) Trost, B. M. *Science* **1991**, *254*, 1471. (b) Anastas, P. T.; Warner, J. C. *Green Chemistry, Theory and Practice;* Oxford University Press: Oxford, U.K., 1998. (c) Clark, J. H. *Green Chem.* **1999**, *1*, 1. (d) Sheldon, R. A. *Green Chem.* **2000**, *2*, G1.

(24) (a) Viswanath, R. P. *Catalysis* **2002**, 227. (b) Sheldon, R. A.; Arends, I. W. C. E.; ten Brink, G. J.; Dijksman, A. *Acc. Chem. Res.* **2002**, *35*, 774.(c) Mallat, T.; Baiker, A. *Chem. Rev.* **2004**, *104*, 3037.

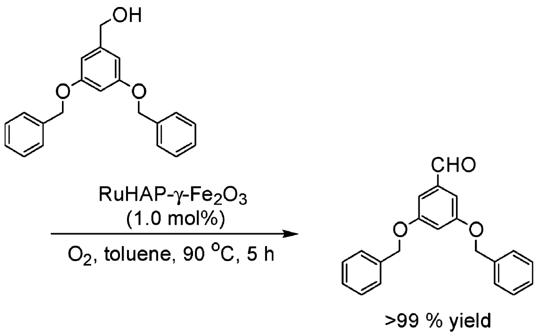

(1)

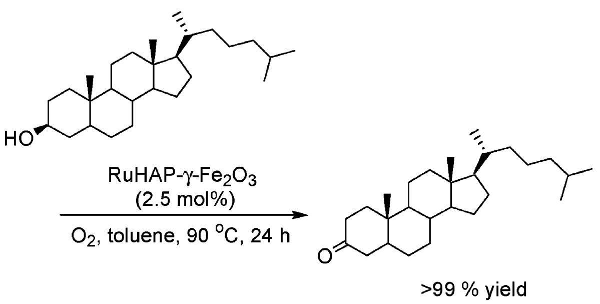

(2)

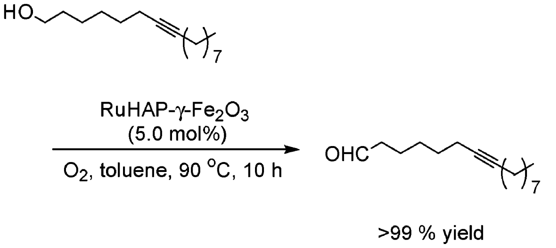

(3)

The characteristic feature of the RuHAP-$\gamma$-$Fe_2O_3$ catalyst is demonstrated by its high initial turnover frequency (TOF). For example, the oxidation of benzyl alcohol using 0.5 mol % of the RuHAP-$\gamma$-$Fe_2O_3$ catalyst afforded benzaldehyde in 98% yield after 1 h; the corresponding TOF based on Ru was 196 $h^{-1}$ (entry 1 in Table 2). Contrastingly, the previously reported RuHAP[4a] and RuCo-HAP[8a] catalysts gave TOFs of 2 and 78 $h^{-1}$, respectively, for this substrate. It is noteworthy that the TOF value achieved by the RuHAP-$\gamma$-$Fe_2O_3$ is significantly higher than those reported for other active Ru catalyst systems, such as $RuCl_2(PPh_3)_3$/TEMPO (80 $h^{-1}$),[25] $Ru/Al_2O_3$ (40 $h^{-1}$),[26] $Ru/CeO_2/CoO(OH)$ (10 $h^{-1}$),[27] Ru−Co−Al−hydrotalcite (9 $h^{-1}$),[28] $RuO_2$/FAU zeolite (8.7 $h^{-1}$),[29] and $(NPr)^+(RuO_4)^-{-}SiO_2$ (1.6 $h^{-1}$).[30] The improved catalytic activity of the RuHAP-$\gamma$-$Fe_2O_3$ may be attributed to the generation of monomeric Ru species with a higher oxidation state. More interestingly, the catalytic activity of the RuHAP-$\gamma$-$Fe_2O_3$ catalyst was substantially accelerated at elevated $O_2$ pressures, as shown in Table 2. The reaction rate for the oxidation of benzyl alcohol under 5 atm of $O_2$ pressure was almost twice as fast as that under atmospheric $O_2$ pressure, in which the TOF value approached 376 $h^{-1}$. Similarly, other benzylic and allylic alcohols could be converted into the corresponding carbonyl compounds with enhanced oxidation rates under 5 atm of $O_2$ pressure. Unfortunately, the oxidations of aliphatic and heterocyclic alcohols were not promoted even under elevated $O_2$ pressure (entries 14, 16, and 20). The above acceleration effect of the RuHAP-$\gamma$-$Fe_2O_3$ catalyst is markedly distinct from that of the RuHAP[4a] and $Ru/Al_2O_3$[26] catalysts, where the initial oxidation rates were found to be independent of the $O_2$ pressure.

**Table 3. Oxidation of Alcohols at Room Temperature by RuHAP-$\gamma$-$Fe_2O_3$ Using $O_2$[a]**

| entry | substrate | mol% | conv. [%][b] | yield [%][b] |
|---|---|---|---|---|
| 1 | 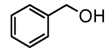 | 1.25 | >99 | 98 |
| 2 | 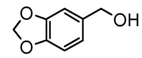 | 4 | >99 | >99 |
| 3 | 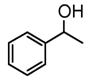 | 1.4 | 94 | 89 |
| 4 | 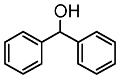 | 1 | 99 | 98 |
| 5 | 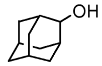 | 2 | >99 | 99 |

[a] Alcohol (0.5−1 mmol), RuHAP-$\gamma$-$Fe_2O_3$ (1−4 mol %), toluene (5 mL), $O_2$ flow, 24 h. [b] Determined by GC using an internal standard technique.

Another important advantage over other catalyst systems is the smooth oxidation of alcohols at room temperature under atmospheric pressure, as summarized in Table 3. It was found that the oxidation of benzyl alcohol proceeded efficiently in the presence of 1.25 mol RuHAP-$\gamma$-$Fe_2O_3$, giving benzaldehyde quantitatively in 24 h (entry 1). 1-Phenylethanol, benzhydrol, and 2-adamantanol also acted as good substrates to provide the corresponding carbonyl compounds (entries 2−4). There have been several previous reports of alcohol oxidation proceeding at room temperature, but these reactions have the disadvantages of long reaction times, low yields, and requirements for additional bases and/or cocatalysts.[31] Our RuHAP-$\gamma$-$Fe_2O_3$ catalyst does not require any additives or cocatalysts to facilitate its efficient catalytic cycle even under mild reaction conditions. We anticipate that this protocol will be of broad interest and applied to thermally unstable alcohols.

Upon completion of the oxidation reaction, the magnetic properties of the RuHAP-$\gamma$-$Fe_2O_3$ can afford a straightforward way of separating the catalyst from the reaction system by applying a permanent magnet externally followed by decantation, as illustrated in Figure 9. The isolated catalyst could be recycled in the oxidation of benzyl alcohol without significant loss of its inherent activity, giving benzaldehyde in 92% yield. Ru K-edge XAFS analysis revealed no

---

(25) Dijksman, A.; Marino-Gonzalez, A.; Payeras, A. M. I.; Arends, I. W. C. E.; Sheldon, R. A. *J. Am. Chem. Soc.* **2001**, *123*, 6826.

(26) Yamaguchi, K.; Mizuno, N. *Chem.—Eur. J.* **2003**, *9*, 4353.

(27) Ebitani, K.; Ji, H.-B.; Mizugaki, T.; Kaneda, K. *J. Mol. Catal., A* **2004**, *212*, 161.

(28) Matsushita, T.; Ebitani, K.; Kaneda, K. *Chem. Commun.* **1999**, 265.

(29) Zhan, B. Z.; White, M. A.; Sham, T. K.; Pincock, J. A.; Doucet, R. J.; Rao, K. V. R.; Robertson, K. N.; Cameron, T. S. *J. Am. Chem. Soc.* **2003**, *125*, 2195.

(30) Ciriminna, R.; Campestrini, S.; Pagliaro, M. *Adv. Synth. Catal.* **2004**, *212*, 161.

(31) (a) Moody, C. J.; Palmer, F. N. *Tetrahedron Lett.* **2002**, *43*, 139. (b) Martin, S. E.; Suarez, D. F. *Tetrahedron Lett.* **2002**, *43*, 4475. (c) Muldoon, J.; Brown, S. N. *Org. Lett.* **2002**, *4*, 1043.

**Figure 9.** Separation of RuHAP-$\gamma$-$Fe_2O_3$ from the reaction mixture under an external magnetic field.

structural changes around the monomeric Ru center in the recovered RuHAP-$\gamma$-$Fe_2O_3$. TEM analysis supports that the size distribution of the $\gamma$-$Fe_2O_3$ nanocrystallites within the HAP matrix remained virtually unchanged even after oxidation. When the catalyst was removed by filtration after ca. 60% conversion at the normal reaction temperature, further treatment of the filtrate under identical reaction conditions did not afford any products. ICP analysis of the filtrate confirmed that the metal contents were determined to be negligible (Ru $<$ 1.6 ppb, Fe $<$ 8 ppb). It can be said that the present reaction undoubtedly proceeds on a solid surface. The above characteristics render the RuHAP-$\gamma$-$Fe_2O_3$ catalyst a pivotal contribution to the development of environmentally acceptable chemical processes, particularly in the industrial and pharmaceutical application of alcohol oxidation.

To help elucidate the pathway of the present reaction, we performed preliminary studies. The catalyst lacking in Ru species, i.e., HAP-$\gamma$-$Fe_2O_3$, was found to be inactive toward alcohol oxidation, indicating that the Ru is an indispensable component of the catalyst. The addition of radical traps, 2,2′,6,6′-tetramethylpiperidine *N*-oxyl (TEMPO) or 2,6-di-tert-butyl-*p*-cresol, had little influence on the oxidation rate of benzyl alcohol. In the case of cyclopropylphenyl carbinol for a radical clock substrate, the oxidation of hydroxyl groups occurred exclusively without skeletal isomerization or carbon−carbon bond cleavage (entry 9 in Table 2). Thus, it was determined that the present catalytic system did not contain free radical intermediates. Monitoring of $O_2$ uptake in the oxidation of benzyl alcohol showed that the ratio of $O_2$ consumed to benzaldehyde was ca. 1:2 during the course of the reaction, suggesting that molecular oxygen was used quantitatively as an oxidant in the oxidative dehydrogenation.[11]

From the above results, it is reasonable to suggest that the RuHAP-$\gamma$-$Fe_2O_3$-catalyzed aerobic alcohol oxidation proceeds via the following mechanism. Initially, a Ru−alcoholate intermediate is formed by the ligand exchange between an alcohol and a surface OH moiety of the RuHAP-$\gamma$-$Fe_2O_3$. The Ru−alcoholate intermediate then undergoes a $\beta$-hydride elimination to produce the corresponding carbonyl compounds and a Ru−H species. Finally, an $O_2$ molecule reacts with the hydride species to afford a Ru−OOH species, followed by the ligand exchange with the alcohol to regenerate the Ru−alcoholate intermediate together with the formation of $O_2$ and $H_2O$. $H_2O_2$ is a probable intermediate in the formation of $O_2$ and $H_2O$.[32] As shown in Figure 8, the FT-EXAFS spectrum of the RuHAP-$\gamma$-$Fe_2O_3$, upon treatment with benzyl alcohol under an Ar atmosphere (sample **B**), showed a decrease in the intensity of the peak attributable to the Ru−O bond at around 1.5 Å compared to that of the fresh RuHAP-$\gamma$-$Fe_2O_3$ (sample **A**). Moreover, after treatment with molecular oxygen of the above, sample **B** recovered the peak intensity (sample **C**). This sequential investigation indicates the formation of shorter Ru−H species under inert conditions and subsequent oxidation with molecular oxygen to form longer Ru−OOH and/or Ru−alcoholate species.

## Conclusions

We have developed RuHAP-$\gamma$-$Fe_2O_3$ as a new multifunctional heterogeneous catalyst. Characterization by means of physicochemical methods revealed that magnetic $\gamma$-$Fe_2O_3$ nanocrystallites with an average diameter of ca. 8.0 nm were dispersed within the HAP matrix. It was also proven that a monomeric Ru cation species containing $Ru^{IV}$ species could be uniformly fixed on the outer HAP surface. The RuHAP-$\gamma$-$Fe_2O_3$ can offer an extremely simple and highly efficient heterogeneous catalyst system for the oxidation of alcohols using molecular oxygen. Recovery of the catalyst was facilely accomplished by external application of a permanent magnet, and the spent catalyst could be recycled without any appreciable loss of activity. The features of the present apatite-based catalysts, such as facile preparation, robust structure, and easy recovery, as well as simple recycling, are particularly desirable for industrial organic synthesis. We expect that the fascinating properties of the HAP-$\gamma$-$Fe_2O_3$ nanocomposite will be further extendable to biomedical fields such as biomolecular separation and targeted drug delivery.

**Acknowledgment.** This work is supported by the Grant-in-Aid for Scientific Research from the Ministry of Education, Culture, Sports, Science, and Technology of Japan (16206078). We thank Dr. Eiji Taguchi (Osaka University) for TEM measurements and Dr. Shotaro Morimoto (Osaka University) for SQUID and $^{57}$Fe Mössbauer measurements.

**Supporting Information Available:** Raman and IR spectra, SEM image, and time profile of $O_2$ uptake. This material is available free of charge via the Internet at http://pubs. acs. org.

CM061388L

---

(32) Attempts to use 30 % aqueous $H_2O_2$ directly as an oxidant did not afford any products and the compound underwent rapid decomposition.